

Fractal Structure in the Collision of Vector Solitons

Jianke Yang and Yu Tan

Department of Mathematics and Statistics, University of Vermont, Burlington, Vermont 05401

(Received 4 April 2000; revised manuscript received 6 July 2000)

We study the collision of two orthogonally polarized and equal-amplitude vector solitons in the nonintegrable coupled nonlinear Schrödinger equations. We show that the separation velocity versus collision velocity graph has a fractal structure. When we zoom into this graph, we get a structure qualitatively identical to the original one. In addition, collision dynamics in the zoomed-in windows is intimately related to that in the original graph. We explain this fractal dependence of the collision by a resonance mechanism between the translational motion of vector solitons and internal oscillations inside a vector soliton.

PACS numbers: 42.65.Tg, 05.45.Df, 05.45.Yv, 42.81.Dp

The coupled nonlinear Schrödinger (NLS) equations arise in a great variety of physical situations. In fiber communication systems, such equations have been shown to govern pulse propagation along orthogonal polarization axes in nonlinear optical fibers [1], and in wavelength-division-multiplexed systems [2]. These same equations also model beam propagation inside crystals or photorefractives [3] as well as water wave interactions [4]. Solitary waves in the coupled NLS equations are often called vector solitons in the literature as they generally contain two components. In all the above physical situations, collision of vector solitons is an important issue. This question has been studied intensively in the past ten years [3,5]. It has been shown that, in addition to passing-through collision, vector solitons can also bounce off each other or trap each other. However, what is still unknown so far is that this collision can be much more complex and regular at the same time. In this paper, we will study the collision of vector solitons and reveal that the separation velocity versus collision velocity graph could have a fractal structure, i.e., when we zoom into this graph, we will get a qualitatively identical copy of the original one. Collision dynamics in the zoomed-in windows is closely related to that in the original window as well. We will explain the existence of this fractal by a resonance mechanism between the translational motion of vector solitons and internal oscillations inside a vector soliton. These internal oscillations are caused by radiation modes, not true internal (shape) modes.

We cast the coupled NLS equations in the birefringent fiber context as [1]

$$i\left(A_Z + \frac{1}{2}V_0A_T\right) + \frac{1}{2}A_{TT} + (|A|^2 + \beta|B|^2)A = 0, \quad (1)$$

$$i\left(B_Z - \frac{1}{2}V_0B_T\right) + \frac{1}{2}B_{TT} + (|B|^2 + \beta|A|^2)B = 0, \quad (2)$$

where A and B are envelopes of the electrical fields in the two orthogonal polarizations of the fiber, T is the time

in the frame moving at the average group velocity of the two polarizations, Z is the propagation distance, V_0 is the inverse-group-velocity difference between the two polarizations, and β is the cross-phase modulational coefficient. All of these variables have been nondimensionalized. In this paper, we consider only collisions of two orthogonally polarized, equal-amplitude vector solitons, as that is the simplest collision configuration, and such collisions arise in applications as well. The initial conditions for such vector solitons can be taken as

$$\begin{aligned} A(T;0) &= \operatorname{sech}\left(T + \frac{1}{2}T_0\right), \\ B(T;0) &= \operatorname{sech}\left(T - \frac{1}{2}T_0\right), \end{aligned} \quad (3)$$

where the soliton amplitudes have been normalized to be one, and T_0 is the initial pulse separation. For these initial conditions, phase differences between the two pulses can be removed. Thus it is not introduced here. We also note that, for these initial conditions, solutions of Eqs. (1) and (2) possess a symmetry: $B(Z, -T) = A(Z, T)$. If there is no cross-phase coupling ($\beta = 0$), each pulse is a NLS soliton which moves at inverse velocity $V_0/2$ or $-V_0/2$. For convenience, we call V_0 the “collision velocity” in this paper. If $\beta = 1$ (Manakov model), the two solitons (3) will also preserve their original velocities, amplitudes, and polarizations after collision as they are orthogonally polarized (if not, amplitudes and polarizations could change after collision) [6]. But when $\beta \neq 0$ or 1 (nonintegrable case), the collision would be very intricate (see below).

We simulated the coupled NLS equations (1) and (2) extensively for $\beta = \frac{2}{3}$, using V_0 as the control parameter. The value $\frac{2}{3}$ is significant as it is the coupling coefficient in linearly birefringent fibers [1]. The initial pulse separation T_0 should be large enough so that the initial pulse overlap is negligible. In our simulations, we used $T_0 = 20$. We employed two different numerical schemes: (1) a third-order split-step method; (2) the pseudospectral method coupled with the 4th order Runge-Kutta integration along the Z direction. Results of these two schemes

were compared closely to guarantee consistency. We also took a large T -interval and used damping conditions at its boundaries. These measures were to ensure that radiation emitted into the far field does not interfere with pulse collisions in the center field. In our simulations, the T interval was 160 units wide. The T -grid points were 1024, and the step size ΔZ was 0.01 (split-step method) and 0.004 (pseudospectral method). We also ran our simulations on selective V_0 values with longer T intervals, wider initial pulse separations, more grid points, and smaller step size ΔZ , and were assured that the results did not change. All our simulations used double precision (about 16 significant digits).

Our simulations identified three collision scenarios: transmission, reflection, and trapping. In a transmission scenario, most of the energy in each pulse passes through; in a reflection scenario, most of the energy is reflected back; in a trapping scenario, the two pulses trap each other and form a single new pulse. If we define the “separation velocity” V as the difference between inverse propagation velocities of the two exit pulses, then the separation velocity is positive in a transmissional collision, negative in a reflectional collision, and zero in a trapping collision. When $V_0 < 0.5512$, we found that the two colliding pulses always trap each other ($V = 0$). When $0.5512 < V_0 < 0.575$ and $V_0 > 0.615$, they always pass through each other ($V > 0$). The most interesting V_0 interval is $[0.575, 0.615]$, where transmissional, reflectional, and trapping collisions all occur in an intertwined way. In this interval, the separation velocity V is plotted in Fig. 1(a). This graph is important in this paper. Several of its features must be noted first. At its left and right ends, there are two “hills” where $V > 0$. Between these hills, there are two prominent intervals where $V < 0$ (“valleys”). The left valley is approximately $[0.5877, 0.5966]$, which is wider. We call it the “W valley.” The right valley, $[0.6006, 0.6033]$, is narrower. We call it the “N valley.” Between these two valleys, there are even narrower “hills” and “valleys.” In addition, intervals of trapping collisions ($V = 0$) scatter around between these hills and valleys. This intertwining structure is the first sign of complexity in these vector-soliton collisions.

The most surprising fact about Fig. 1(a) is that, when we zoom into this graph, we get structures similar to the original one. To show this, we zoom into the tiny V_0 window $[0.60366, 0.60385]$ lying between the N valley and the rightmost hill. This window is marked by two vertical lines in Fig. 1(a) (the two lines are so close by that they are almost indistinguishable). This window, when enlarged, is shown in Fig. 1(b). But Fig. 1(b) is qualitatively the same as Fig. 1(a). In Fig. 1(b), the graph also has two “hills” at the left and right ends. In between, there are also two prominent valleys which are the counterparts of the W valley and N valley in Fig. 1(a). The W valley here, $[0.603717, 0.603745]$, is to the left, and the N valley, $[0.6037738, 0.6037854]$, is to the right, just as in Fig. 1(a).

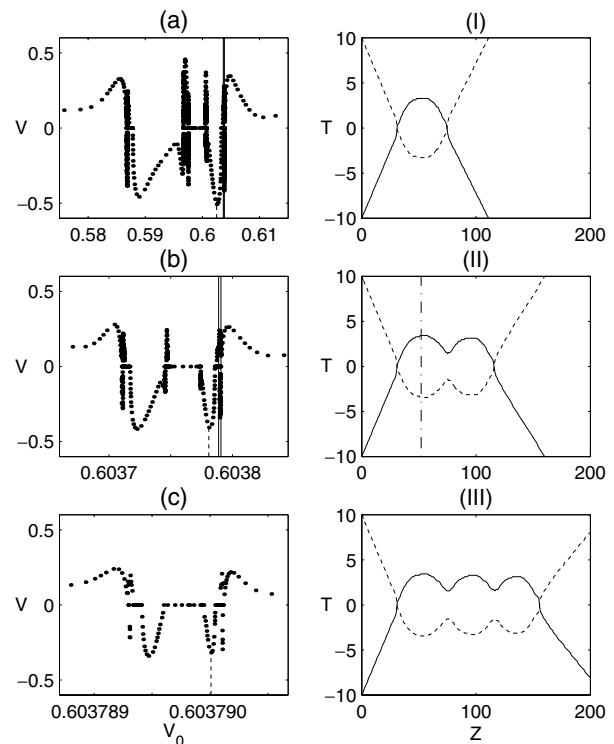


FIG. 1. Fractal structure and collision dynamics of vector solitons. In the left column are graphs of separation velocity V versus collision velocity V_0 . (b) and (c) are successive amplifications of (a) in intervals marked by vertical solid lines. In the right column are collision dynamics of vector solitons with velocities V_0 at the bottoms of the N valleys in the left column (marked by vertical dashed lines). Specifically, in (I), $V_0 = 0.6025$; in (II), $V_0 = 0.603781$; in (III), $V_0 = 0.6037901$. Plotted here are positions of maximum $|A|$ and $|B|$ amplitudes at each distance Z (solid for $|A|$ and dashed for $|B|$).

Between these valleys, narrower hills and valleys as well as trapping intervals can be found intertwined too. Some differences also exist between Figs. 1(a) and 1(b). The most notable difference is that Fig. 1(b) has even narrower hills and valleys between its W valley and N valley. Another difference is that the vertical heights of hills and valleys in Fig. 1(b) are generally lower than their counterparts in Fig. 1(a). But these differences are relatively minor.

The surprise does not stop here. When we zoom into the same relative position in Fig. 1(b) as in Fig. 1(a), we get yet another structure which is similar to Figs. 1(a) and 1(b). Specifically, we zoom into the narrow interval $[0.6037887, 0.6037907]$, which lies between the N valley and the rightmost hill of Fig. 1(b), the same relative position as the zoomed-in window in Fig. 1(a). This window is marked in Fig. 1(b) by two vertical lines. The amplified window is shown in Fig. 1(c). This graph also has two hills at the two ends of the interval. In between, a wider valley is to the left (W valley), and a narrower valley is to the right (N valley), just as in Figs. 1(a) and 1(b). These three graphs in Fig. 1 indicate that the structure in Fig. 1(a) is a fractal. We would like to remind the reader

that the length of the V_0 interval in Fig. 1(c) is 2×10^{-6} . On such a fine scale, the collision still has a rich structure, which is truly remarkable. Figure 1(c) can be zoomed in even further. But numerical simulations then become more sensitive, and greater accuracy would be required.

What is described above is the geometrical structure of the separation velocity graph. Dynamically, we have found that collisions in Figs. 1(a) and its zoomed-in windows [Figs. 1(b) and 1(c)] are intimately related. Specifically, collisions at the same relative positions in these figures follow simple and clear patterns. To demonstrate, we select the bottom points of N valleys in these graphs, i.e., $V_0 = 0.6025$, $0.603\,781$, and $0.603\,790\,01$, respectively [marked in Figs. 1(a)–1(c) by dashed vertical lines]. In each case, the collision is reflectional ($V < 0$). When we plot the positions of maximum $|A|$ and $|B|$ amplitudes at each distance Z (solid for $|A|$ and dashed for $|B|$), we get Figs. 1(I)–1(III), respectively. In the first graph, Fig. 1(I), the colliding pulses first pass through each other, reach finite separation, stop, return, and pass through each other the second time, and then separate. In Fig. 1(II), the colliding pulses first pass through each other, reach finite separation, stop, oscillate around its position once, then return and pass the second time and separate. In Fig. 1(III), the collision is similar to Figs. 1(I) and 1(II) except that the two pulses oscillate twice around their positions between the two passes. The clear patterns in these collisions are amazing. At other points of the same relative position in Figs. 1(a)–1(c), collisions show similar patterns. Specifically, collision in the zoomed-in window is that, after the first pass, the pulses oscillate one more time around their positions than in the original window. The rest of the collision pattern remains the same. These patterns indicate that collisions in the fractal structure of Fig. 1(a) can be classified and understood according to the relative positions of V_0 in this fractal. This is analogous to the quadratic map $f(z) = z^2 + c$, where the shape of its Julia set can be predicted and classified by the location of parameter c in the Mandelbrot set [7]. We have also observed that distances between two passes in Figs. 1(I)–1(III) are roughly 43.6, 84.7, and 124.6, respectively. Collision of the same nature as Figs. 1(I)–1(III) but with four “bumps” occurs at $V_0 = 0.603\,790\,109\,1$. This point would be the bottom of the next N valley when we zoom into the narrow window between the N valley and rightmost hill of Fig. 1(c). The distance between two passes at this velocity is about 162.2. An interesting fact is that these collision distances Z_c can be fit nicely by the formula

$$\omega Z_c = \delta + 2\pi n, \quad (4)$$

where $\omega = 0.158$, $\delta = 0.68$, and n is the number of bumps. The relative error of this fit is less than 1%. Similar relations have been found in kink-antikink collisions as well [8,9]. In that context, ω was the internal-mode frequency for the kink/antikink.

An important question is how to theoretically explain the fractal structure and collision dynamics in Fig 1. Here it is instructive to recall that a similar fractal structure has been discovered in kink-antikink collisions in nonintegrable sine-Gordon type equations [8,9]. In such systems, the fractal was explained by a resonance between the translational motion of the kink/antikink and the internal (shape) mode of the kink/antikink. This internal mode is a discrete eigenfunction with nonzero eigenvalue in the linearized system around a kink/antikink. Could a similar mechanism be responsible for the present fractal?

To answer this question, we first discuss the internal dynamics of a perturbed vector soliton. This subject has been studied in great detail in [10,11]. It has been shown that this dynamics is dominated by two oscillations: one is the oscillation of position separation between two components of the vector soliton; the other one is an in-phase width oscillation (the third, out-of-phase width oscillation is unstable and rearranges itself into the in-phase width oscillation mode [10]). For $0 < \beta < 1$ and the polarization angle of a vector soliton falling in a certain interval centered at 45° , the oscillation of position separation is caused by a true internal mode which lies in the gap of the continuous spectrum in the linearized system around the vector soliton. In that case, the frequency of position oscillation is the eigenvalue of the internal mode, and this oscillation is the most persistent. In other cases, the internal mode merges into the edge of the continuous spectrum of the linearized system. In this situation, the positional oscillation is caused by radiation modes. It is less persistent, but still fairly robust. The frequency of this position oscillation is just the edge point value of the continuous spectrum. This fact is not obvious. But it can be inferred from the work [12] for the single NLS equation, from the work [11] on positional oscillations inside a vector soliton, and from our numerical experiments. This fact highlights the importance of this edge point of the continuous spectrum for positional oscillations. The in-phase width oscillation of a vector soliton is always caused by radiation modes, and its frequency is the edge point of the continuous spectrum for the larger-amplitude component (this is analogous to the width oscillation of a single NLS soliton [12]). This oscillation is even less robust. All the above facts have been verified independently by our own numerics.

Could the fractal structure in Fig. 1 be caused by a resonance between the translational motion of a vector soliton and internal oscillations described above? Let us examine a representative case shown in Fig. 1(II) in detail below. After the first pass, the two solitons reach maximum separation 6.8 when $Z_0 \approx 52$ [this Z_0 location is shown in Fig. 1(II) as a vertical dash-dotted line]. At this instant, we found that the solutions A and B could be approximated by a superposition of two vector solitons with zero velocities, nearly zero phase differences, and component amplitudes (0.774, 0.501) and (0.501, 0.774), respectively. The

polarizations of these vector solitons are 33° and 57° . We note that when the soliton separation in Fig. 1(II) is not maximal, the two-vector-soliton approximation would not be as good. It has been shown in [11] that, when $\beta = 2/3$, only vector solitons with polarizations between 41.1° and 48.9° allow internal modes. Thus, the two vector solitons above do not support true internal modes. The propagation constants (wave numbers) for the larger and smaller components of these vector solitons were found to be 0.388 and 0.314, respectively. Thus the edge points of the continuous spectrum for the linearized system around such a vector soliton are ± 0.314 , and the edge points of the continuous spectrum for the larger wave component are ± 0.388 . In view of the discussions in the previous paragraph, we see that the frequency of positional oscillation in each vector soliton is the continuum edge point 0.314, while the in-phase width oscillation has frequency 0.388. Since the two vector solitons are almost in-phase, they attract each other. This causes the translational motion of vector solitons seen in Fig. 1(II). The frequency of this translational motion is $\omega = 0.158$ [see Eq. (4)].

A fact we notice is that the positional oscillation frequency, 0.314, is almost exactly twice the translational frequency ω . This suggests that there is indeed a resonance present in this collision. This resonance appears to be between the translational motion of vector solitons and positional oscillations of two components inside each vector soliton. In the present case, this position oscillation is caused by radiation modes, not internal modes. But it is analogous to the oscillation caused by internal modes when such modes do exist [11]. We also detected signs of in-phase width oscillations at frequency 0.388 during this collision. This frequency is close to 2ω . Thus width oscillations may also play a significant role in resonant collisions.

The above discussion was made for Fig. 1(II). When we examined Figs. 1(I) and 1(III), we found the same resonance mechanism operating. This shows that collision dynamics in Fig. 1 could be explained by a resonance mechanism between the translational motion of vector solitons and internal oscillations inside each vector soliton.

In Figs. 1(a)–1(c), we zoomed into the position between the N valley and the rightmost hill. If we zoom into certain other positions of the fractal (but not any position), we will obtain other types of fine structures. Collision dynamics in these zoomed-in windows is also closely related to that in the original structure, but in a way different from Figs. 1(I)–1(III). A detailed report of these results will be given elsewhere.

As we have mentioned above, a similar fractal structure has been reported for kink-antikink collisions in the ϕ^4 model [9]. However, the resonance in the present model is between the translational motion and radiation modes, while the resonance in ϕ^4 is between the translational

motion and a true localized internal mode. Since radiation modes exist for all conservative evolution equations, while internal modes exist only for some of them, we see that the present resonance mechanism for fractal structures is more universal. Recently, an interesting Cantor fractal was reported for soliton breakups due to a sequence of abrupt changes in the dispersion coefficient [13]. That fractal is of a different nature as the underlying mechanism is different.

In conclusion, we have reported a fractal structure in solitary-wave collisions for the coupled NLS equations. This structure lies in the separation velocity versus collision velocity graph. We have explained this structure by a resonance between the translational motion of vector solitons and internal oscillations inside a vector soliton. These results could have important applications to physical systems where vector-soliton collisions arise. They also have direct ramifications to solitary wave collisions in other physical systems. The experimental verification of these results is quite feasible.

The authors thank Dr. R. Knapp for help with the numerics. This work was supported in part by AFOSR under Contract No. USAF F49620-99-1-0174, and by NSF under Grant No. DMS-9971712.

-
- [1] C. R. Menyuk, *IEEE J. Quantum Electron* **23**, 174 (1987).
 - [2] G. P. Agrawal, *Nonlinear Fiber Optics* (Academic Press, San Diego, 1995).
 - [3] C. Anastassiou *et al.*, *Phys. Rev. Lett.* **83**, 2332 (1999).
 - [4] D. J. Benney and A. C. Newell, *J. Math. Phys.* **46**, 133–139 (1967).
 - [5] B. A. Malomed and S. Wabnitz, *Opt. Lett.* **16**, 1388 (1991); J. Yang, *Phys. Rev. E* **59**, 2393 (1999); C. Sophocleous and D. F. Parker, *Opt. Commun.* **112**, 214 (1994).
 - [6] S. V. Manakov, *Sov. Phys. JETP* **38**, 248–253 (1974).
 - [7] H. O. Peitgen and P. H. Richter, *The Beauty of Fractals* (Springer-Verlag, Berlin, 1986).
 - [8] D. K. Campbell, J. F. Schonfeld, and C. A. Wingate, *Physica (Amsterdam)* **9D**, 1 (1983); D. K. Campbell, M. Peyrard, and P. Sodano, *Physica (Amsterdam)* **19D**, 165 (1986).
 - [9] P. Anninos, S. Oliveira, and R. A. Matzner, *Phys. Rev. D* **44**, 1147–1160 (1991).
 - [10] T. Ueda and W. L. Kath, *Phys. Rev. A* **42**, 563 (1990); D. J. Kaup, B. A. Malomed, and R. S. Tasgal, *Phys. Rev. E* **48**, 3049–3053 (1993); B. A. Malomed and R. S. Tasgal, *Phys. Rev. E* **58**, 2564–2575 (1998).
 - [11] J. Yang, *Stud. Appl. Math.* **98**, 61–97 (1997); D. E. Pelinovsky and J. Yang (to be published).
 - [12] M. W. Chbat *et al.*, *J. Opt. Soc. Am. B* **10**, 1386 (1993); E. A. Kuznetsov, A. V. Mikhailov, and I. A. Shimokhin, *Physica (Amsterdam)* **87D**, 201–215 (1995).
 - [13] S. Sears, M. Soljacic, M. Segev, D. Krylov, and K. Bergman, *Phys. Rev. Lett.* **84**, 1902 (2000); M. Soljacic, M. Segev, and C. R. Menyuk, *Phys. Rev. E* **61**, 1048 (2000).